CASE 2: URANS APPLICATION WITH CFL3D

C. L. Rumsey

Computational Modeling & Simulation Branch, NASA Langley Research Center, Hampton, VA 23681-2199

Solution Methodology

This case was run using CFL3D, a multi-zone Reynolds-averaged Navier-Stokes code developed at NASA Langley [1]. It solves the thin-layer form of the Navier-Stokes equations in each of the (selected) coordinate directions. It can use 1-to-1, patched, or overset grids, and employs local time step scaling, grid sequencing, and multigrid to accelerate convergence to steady state. In time-accurate mode, CFL3D has the option to employ dual-time stepping with subiterations and multigrid, and it achieves second order temporal accuracy.

CFL3D is a finite volume method. It uses third-order upwind-biased spatial differencing on the convective and pressure terms, and second-order differencing on the viscous terms; it is globally second-order spatially accurate. The flux difference-splitting (FDS) method of Roe is employed to obtain fluxes at the cell faces. It is advanced in time with an implicit three-factor approximate factorization method.

Model Description

For this test case, two different turbulence models have been run to date. The first is the one-equation Spalart-Allmaras model (SA) [2], and the second is the two-equation shear-stress transport model of Menter (SST) [3, 4]. These are both linear eddy-viscosity models that make use of the Boussinesq eddy-viscosity hypothesis. The equations describing these two models can be found in their respective references.

In CFL3D, the models are implemented uncoupled from the mean-flow equations. They are solved using a three-factor implicit approximate factorization approach. The advection terms are discretized with first-order upwind differencing. The production source term is solved explicitly, while the advection, destruction, and diffusion terms are treated implicitly.

Implementation and Case Specific Details

In this flow, a synthetic jet issues into a turbulent boundary layer through a circular orifice of diameter 6.35 mm in the floor. The flow is characterized by a forcing frequency of 150 Hz, with a maximum discharge vertical velocity of approximately $1.25U_\infty$. The approach boundary layer thickness is somewhat greater than 20 mm, the freestream Mach number is $M = 0.1$, and the Reynolds number is approximately $\mathrm{Re} = 14160$ per orifice diameter.

The grid used was the supplied structured grid number 1 (which contains 7-zones connected in a 1-to-1 fashion, and approximately 4.09 million grid points), as well as a medium-level grid made from the fine grid by extracting every-other point in each coordinate direction. The SA model was solved on both the fine and medium grids, whereas the SST model was only solved on the medium grid.

The time step chosen was one that yielded 720 time steps per cycle of the forcing frequency. For the SA model, 5 subiterations were employed per time step. For the SST model, however, a large instability was noted when 5 subiterations were employed. This instability showed up as a series of un-physical oscillations in the flowfield variables at given points in space during part of the cycle. By increasing the number of subiterations to 10, the level of this instability decreased, but it did not go away. See for example, Fig. 1, which shows the vertical (W) velocity component as a function of phase 1D downstream of the center of the

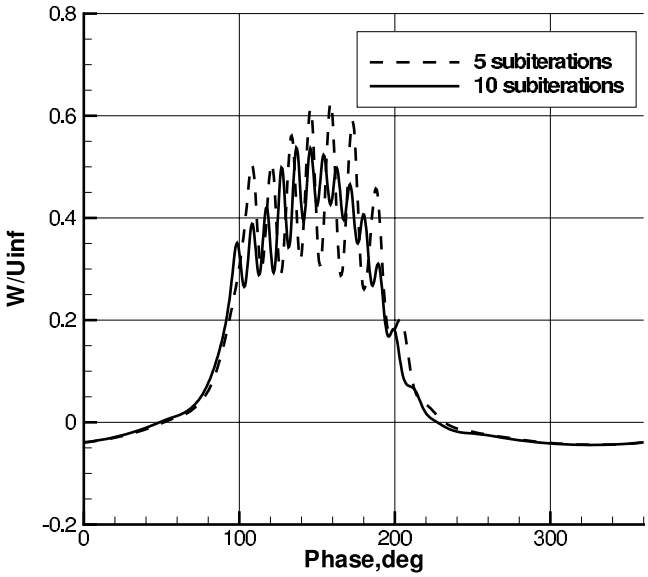

Figure 1: Effect of subiterations on result using SST at x=57.15 mm, z=10 mm (1D downstream), medium grid.

orifice, at z=10 mm above the floor. Therefore, the current SST results should be considered as incomplete; future work will address eliminating the instability.

The boundary conditions were as follows. At the tunnel floor as well as on the inner lip of the orifice and upper wall of the cavity, solid wall adiabatic boundary conditions were applied. The side walls of the cavity were modeled as slip walls, and the bottom surfaces of the cavity employed a time-dependent boundary condition. In other words, the moving diaphragm was modeled on the stationary grid through the use of a boundary condition that imposed a vertical velocity in a sinusoidal manner. (Note that the bottom of the cavity in the supplied grid modeled both the elastic diaphragm as well as the solid plate glued to its center. The time-dependent boundary condition was applied both on the part modeling the elastic diaphragm as well as on the part modeling the solid plate.) The time-dependent boundary condition set the velocity components as follows:

$$U = 0 \qquad V = 0 \qquad W = [(\rho W)_{\max}/\rho] cos(2\pi F t) \tag{1}$$

where F is the frequency and t is the time. With this boundary condition, the density and pressure are extrapolated from the interior of the domain. The $(\rho W)_{\max}$ was chosen by trial and error in order to achieve an approximate match of the vertical velocity component at the outflow of the orifice with the experiment (the final value used was $(\rho W)_{\max} = 0.0008 \rho_\infty a_\infty$, where a_∞ is the reference speed of sound). The resulting W and U components of velocity at the orifice exit can be seen in Figs. 2 and 3. Note that use of the current boundary condition fails to capture the sharp peak in W and the additional hump on the downstroke. Also, it should be noted that the experimental data exhibited significant side (V-component) velocities during the cycle at this location, whose cause has not been accounted for. The current CFD method makes no attempt to duplicate this V-velocity component. Also shown in these figures is the effect of fine vs. medium grids, which is very small at this point in the flowfield.

The supplied grid extends .0508 m upstream of center of the orifice, and .1016 m downstream of the center of the orifice. Its height is .076 m above the floor, and its width extends from y=-.038 m to +.038 m

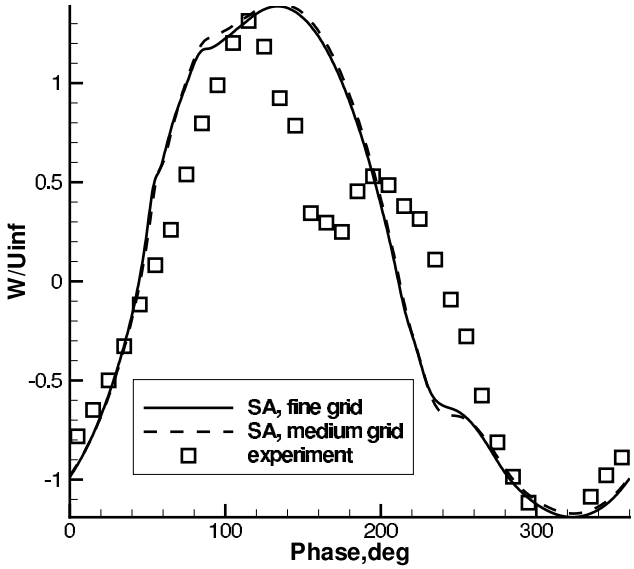

Figure 2: Vertical velocity component at the orifice exit.

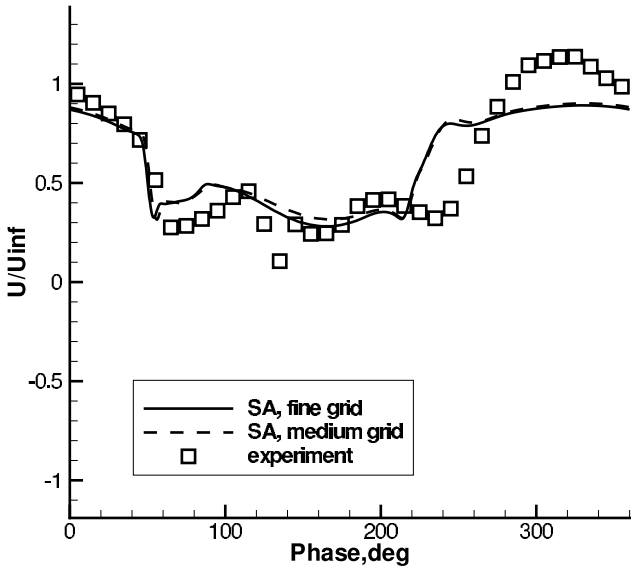

Figure 3: Streamwise velocity component at the orifice exit.

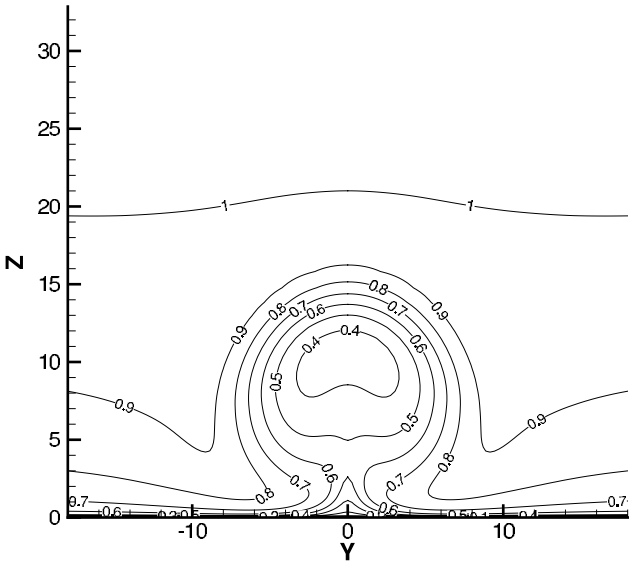

Figure 4: Contours of U/U_∞ at x=76.2 mm (4D downstream), phase=$200°$, SA on fine grid.

(total width of .076 m). Note that this height and width are smaller than the wind tunnel height (approx .249 m) and width (.381 m). The boundary conditions at the top, side, and downstream faces of the grid in the tunnel are a farfield Riemann-type. At the upstream face in the tunnel, the density and velocity components are specified in order to approximately match the experimental boundary layer thickness, and the turbulence data is specified in order to approximate a fully-developed turbulent boundary layer in its $\overline{u'w'}$ component. The pressure at the inflow is extrapolated from the interior of the domain.

Examples of the effects of grid and turbulence model can be seen in Figs. 4, 5, and 6, at phase=$200°$ in the plane 4D downstream (x=76.2 mm). SA on the fine grid yields a somewhat rounder structure than SA on the medium grid, but overall the results are very similar. The differences between the SA and SST models (on the medium grid) are also relatively minor, with the SST model producing a thinner and taller structure.

References

[1] Krist, S. L., Biedron, R. T., and Rumsey, C. L., "CFL3D User's Manual (Version 5.0)", NASA TM-1998-208444, June 1998.

[2] Spalart, P. R., and Allmaras, S. R., "A One-Equation Turbulence Model for Aerodynamic Flows," *La Recherche Aerospatiale*, No. 1, 1994, pp. 5–21.

[3] Menter, F. R., "Two-Equation Eddy-Viscosity Turbulence Models for Engineering Applications," *AIAA Journal*, Vol. 32, No. 8, 1994, pp. 1598–1605.

[4] Menter, F. R., Rumsey, C. L., "Assessment of Two-Equation Turbulence Models for Transonic Flows," AIAA Paper 94-2343, Colorado Springs, CO, 1994.

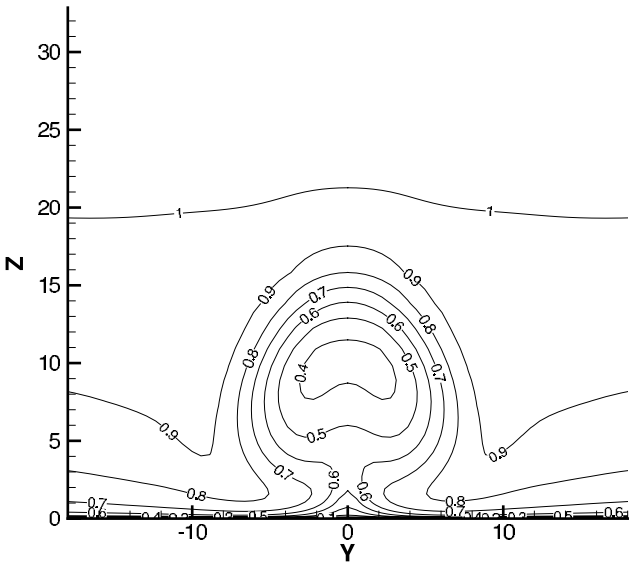

Figure 5: Contours of U/U_∞ at x=76.2 mm (4D downstream), phase=$200°$, SA on medium grid.

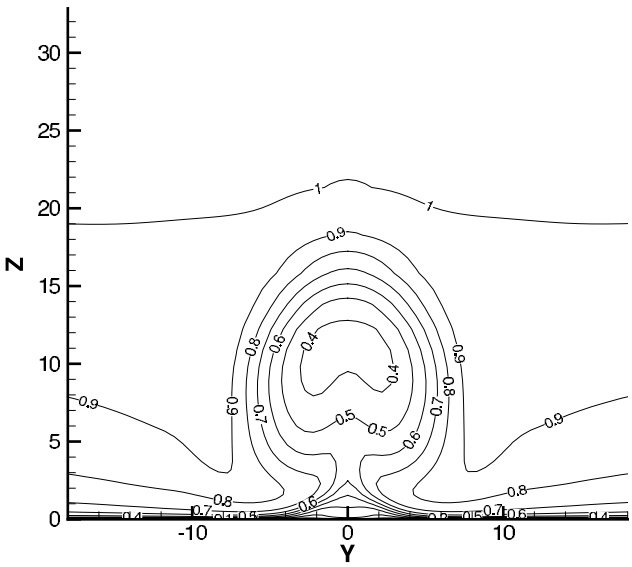

Figure 6: Contours of U/U_∞ at x=76.2 mm (4D downstream), phase=$200°$, SST on medium grid.